

^{19}F -MRS/ ^1H -MRI dual-function probe for detection of β -galactosidase activity†

Cite this: *Chem. Sci.*, 2013, **4**, 2132Jian-Xin Yu,^{*a} Vikram D. Kodibagkar,^b Li Liu,^c Zhongwei Zhang,^a Li Liu,^a Jennifer Magnusson^a and Yuting Liu^d

Because of the importance of *lacZ* gene in various applications ranging from molecular biology to clinical trials, the development of non-invasive bimodal techniques for improving precision and accuracy to assay gene expression has attracted much attention. In this paper, we propose a dual-function probe for synergistic combination of ^{19}F -MRS/ ^1H -MRI to simultaneously detect β -gal activity. Based on this strategy, we have designed, synthesized and characterized a series of ^{19}F -MRS/ ^1H -MRI reporters, and demonstrated the feasibility of 1-O-(β -D-galactopyranosyl)-3-fluorocatechol **MGD-3-FCAT** for assessing β -gal activity in solution and *in vitro* with *lacZ* transfected tumor cells as well, by the characterization of β -gal responsive ^{19}F -chemical shift changes $\Delta\delta_{\text{F}}$, hydrolytic kinetics, and T_1 , T_2 relaxation mapping.

Received 28th July 2012
Accepted 25th February 2013

DOI: 10.1039/c3sc21099e

www.rsc.org/chemicalscience

Introduction

As a reporter, the *lacZ* gene encoding β -galactosidase (β -gal) has been widely applied in molecular biology, small animal investigations and clinical trials, including assays of clonal insertion, transcriptional activation and protein expression, as well as protein interaction.^{1–3} Therefore, its detection has been exploited with techniques from colorimetric,⁴ fluorescence,^{5–7} chemiluminescence,^{8,9} positron emission tomography or single-photon emission computed tomography,^{10,11} to magnetic resonance imaging (MRI)^{12–17} and ^{19}F -MRS/MRI.^{18–26}

Comparatively, ^1H -MRI is a superior imaging modality in living systems because it is non-invasive, able to differentiate between soft tissues, and has high lateral and depth resolutions. Currently, ^1H -MRI is widely applied for medical diagnosis, and becomes one of the most promising techniques for investigation of physiological events.²⁷ However, contrast agent enhanced ^1H -MRI often suffers from low contrast-to-noise ratio because of the large background signals. To avoid this limitation, ^{19}F -MRI recently has been attracting considerable attention as an alternative technique, since the ^{19}F nucleus has a

high gyromagnetic ratio ($\gamma = 40.05 \text{ MHz T}^{-1}$), 100% natural isotopic abundance, large chemical-shift dispersion, importantly, essentially no intrinsic ^{19}F signals detectable in living tissue and thus no interference from background signals.^{18,24} So far aside from the *lacZ* gene ^{19}F -MRS/MRI reporters, there have been varieties of other functional ^{19}F -NMR probes developed for studies of diverse biological events.^{28–38}

However, unlike the mechanism of ^1H -MRI, which visualizes numerous water molecules around the probes, ^{19}F -MRI intensity is only attributed from the probe signals or content, resulting in poor sensitivity,^{18,24,37} which is the major obstacle of this technique for further applications. Different from ^{19}F -MRI, ^{19}F -MRS has been widely involved in *in vivo* studies on drug absorption, distribution, metabolism and excretion for reasons of its favorable MR properties, simplicity and high sensitivity.³⁹ In this paper, we propose a novel dual-function probe for synergistic combination of ^{19}F -MRS/ ^1H -MRI to detect β -gal activity, in which ^{19}F -MRS recognizes its presence and progression by defining the ^{19}F chemical shift change and hydrolytic kinetics, whereas ^1H -MRI reveals its location and magnitude by high spatial resolution and 3-dimensional anatomical details.

Probe design

Cancer cells exhibit increased uptake and utilization of more Fe^{3+} because of their rapid replication.^{40,41} By chelating with cancer cellular Fe^{3+} to reduce its levels, various critical cellular processes dependent on Fe^{3+} in cancer are disrupted. Through this mechanism, chelators are employed to inhibit tumor growth as iron chelation therapy. Pyridoxal isonicotinoylhydrazone (**PIH**), salicylaldehyde benzoylhydrazone (**SBH**), salicylaldehyde isonicotinoylhydrazone (**SIH**) and

^aDepartment of Radiology, The University of Texas Southwestern Medical Center at Dallas, 5323 Harry Hines Blvd., E6.118, Dallas, Texas 75390-9058, USA. E-mail: Jian-Xin.Yu@UTSouthwestern.edu; Fax: +1 214-648-4538; Tel: +1 214-648-2716

^bCurrently at School of Biological and Health Systems Engineering, Arizona State University, Tempe, AZ 85287-9709, USA

^cXinjiang Institute of Chemistry and Physics, Chinese Academy of Sciences, 40 Beijing South Road, Urumqi, Xinjiang 830011, China

^dDepartment of Chemistry, Xinjiang University, 14 Victory Road, Urumqi, Xinjiang 830046, China

† Electronic supplementary information (ESI) available: Fig. S1–S5, syntheses of ligands and their corresponding Fe-complexes as well as molecular characterization of 3- and 4-FCAT β -D-galactopyranosides. See DOI: 10.1039/c3sc21099e

salicylaldehyde nicotinoylhydrazone (**SNH**) (Fig. 1 and S1†) are in clinical trials for the treatment of various metastatic and solid cancers, and fluorinated chelators have shown pronounced anticancer activities, even more effective than each of their parent chelators.^{40,41}

From the structural similarities of the Fe-complexes of the clinically applied chelators and the known Fe-based ¹H-MRI contrast agents,⁴² we speculated that the clinically applied Fe-chelators could act as Fe-based ¹H-MRI contrast agents. When using fluorinated chelators as aglycons, their β-D-galactosides will work as prodrugs, in which the sugar residue β-D-galactopyranosyl will act as a carrier and masking unit. Upon cleavage at a *lacZ* transfected tumor, the blocked fluorinated chelators will be *lacZ* (or β-gal)-specifically released and activated to capture the tumor abundant Fe³⁺. The *in situ* formed paramagnetic Fe-complexes will (1) generate ¹H-MRI contrast and (2) localize and accumulate ¹⁹F-MRS signals at the site of β-gal activity. Fig. 2 illustrates the design principle of ¹⁹F-MRS/¹H-MRI dual-function probe for detecting β-gal activity, using SBH as a model chelator.

However, the paramagnetic metal ions like Gd³⁺, Fe³⁺ and Mn²⁺ can shorten the relaxation time of ¹⁹F nucleus by the paramagnetic relaxation enhancement (PRE) effect,⁴³ in which the distance between the ¹⁹F nucleus and paramagnetic center is vital for the PRE modulation.⁴⁴ Based on this mechanism, Kikuchi *et al.* developed off-on switching ¹⁹F-MRI probes such as Gd-DFP-Gal, Gd-DOTA-DEVD-Tfb, Gd-DOTA-DEVD-AFC and Gd-FC-Lac to detect β-gal, protease or β-lactamase activities *in vitro*.^{26,34,35}

In contrast to Gd³⁺ with very strong relaxivity, Fe³⁺ has a much shorter electronic relaxation time, and limits the relaxation enhancing efficiency on ¹⁹F nucleus. Importantly, other than Gd³⁺-complexes which are isotropic electron systems, the Solomon-Bloembergen theory assumes that Fe³⁺-complexes represent anisotropic paramagnetic systems, in which the Fe³⁺-complex PRE interaction vectors are rigid in the molecular frame.⁴³ This offers us a possibility of constructing a novel probe with an ¹⁹F-atom closer to the paramagnetic Fe³⁺ center in a conjugated molecule as designed in Fig. 2, which is expected to have a large ¹⁹F-NMR chemical shift difference upon β-gal cleavage, but without an Fe³⁺-¹⁹F PRE effect.

This concept of probe design is based on tumor biology and synergizes the advantages of ¹⁹F-MRS and ¹H-MRI. The mechanism proceeds in the β-gal responsive “turn-on” way to simultaneously generate ¹H-MRI contrast and ¹⁹F-MRS signal shift, which are selectively and specifically confined and gathered at the site of β-gal activity, offering increases of the magnitudes of both signals and reliability of detection, as well as better precision and accuracy.

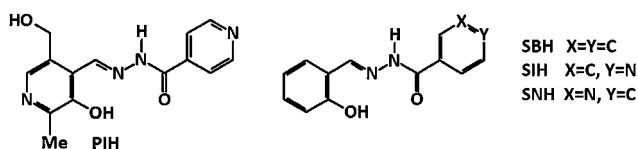


Fig. 1 Structures of PIH, SBH, SIH and SNH.

Results and discussion

¹H-MRI verification

The clinically applied tridentate chelators PIH, SBH, SIH and SNH, and their corresponding 2 : 1 Fe-complexes [Fe(PIH-H)₂]⁺ (PIH/Fe³⁺), [Fe(SBH-H)₂]⁺ (SBH/Fe³⁺), [Fe(SIH-H)₂]⁺ (SIH/Fe³⁺), [Fe(SNH-H)₂]⁺ (SNH/Fe³⁺) were synthesized according to the described methods (see ESI†).^{40,41} T₁/T₂/T₂*-weighted ¹H-MRI evaluations were investigated by using a spin echo pulse sequence at varying repetition times (TRs) and echo times (TEs). As we expected, the results showed that the complexes PIH/Fe³⁺, SBH/Fe³⁺, SIH/Fe³⁺ or SNH/Fe³⁺ each produced a substantial T₁-weighted contrast (Fig. 3), which opens a new era of an Fe-depletion complex functioning as a ¹H-MRI agent, and also suggests a potential for clinical theranostic application.

¹⁹F-MRS/¹H-MRI dual-function confirmation

Following the strategy described in Fig. 2, we firstly prepared tridentate 2-hydroxyl-5-fluorobenzaldehyde benzoylhydrazone (**p-FSBH**) according to the previously described method (see ESI†).^{25,40,41} ¹⁹F-NMR tests showed that **p-FSBH** in 1 : 1 (v/v) DMSO/PBS (0.1 M, pH = 7.4) at 25 °C gave a single narrow ¹⁹F-MRS signal with respect to sodium trifluoroacetate (NaTFA, δ_F = 0 ppm) at δ_F = −49.60 ppm, which was attenuated to vanished very quickly upon the addition of a half equivalent ferric ammonia citrate (FAC), due to the strong intramolecular PRE effect on the 5-¹⁹F nucleus from the *in situ* generated paramagnetic 2 : 1 Fe-complex [Fe(**p-FSBH-H**)₂]⁺ (**p-FSBH/Fe³⁺**), it indicates that the ¹⁹F nucleus in the para-position to 2-hydroxyl is still in the range of PRE. The distance from ¹⁹F to paramagnetic Fe³⁺ *r* = 7.01 Å was calculated from the computed minimized energy conformation of Fe-complex **p-FSBH/Fe³⁺** using Chem3D 8.0 (MM2 as the force-field) and Visual Molecular Dynamics (VMD 1.9). The T₁-weighted images showed that the contrast enhancement of Fe-complex **p-FSBH/Fe³⁺** in Fig. 4 was similar to **SBH/Fe³⁺** in Fig. 3. However, when the ¹⁹F-atom was introduced in the para-position to benzoylhydrazone (**SBHF-p**) with the distance to paramagnetic Fe³⁺ of *r* = 8.10 Å, its ¹⁹F-MRS signal intensity was reduced by 22% from a sharp peak to a broad singlet at δ_F = −32.66 ppm upon the formation of Fe-complex [Fe(**SBHF-p-H**)₂]⁺ (**SBHF-p/Fe³⁺**). Also, significant contrast change in T₁-weighted MR images was observed (Fig. 5). The identical T₁-weighted images compared with the prepared [Fe(**SBHF-p-H**)₂]⁺ (**SBHF-p/Fe³⁺**) confirmed the attribution to the intramolecular Fe³⁺-¹⁹F PRE effect.

Inspired by these results, we turned to the bidentate catechol analogues, which also are the most widely used Fe³⁺ chelators,^{40,41} and identified recently as the endogenous ligands for siderocalin to deliver Fe³⁺ to the kidney.⁴⁵ Catechol moieties possess a high affinity for Fe³⁺ to form thermodynamically stable 1 : 3 Fe³⁺-complexes at physiological pH, and discriminately coordinate to other biologically critical metal ions such as Zn²⁺, Cu²⁺ and Ca²⁺. This unique specificity is very essential in the development of clinically useful metal-ligand systems. Moreover, catecholate ligands are of particular interest in the development of Fe³⁺-based ¹H-MRI contrast agents because

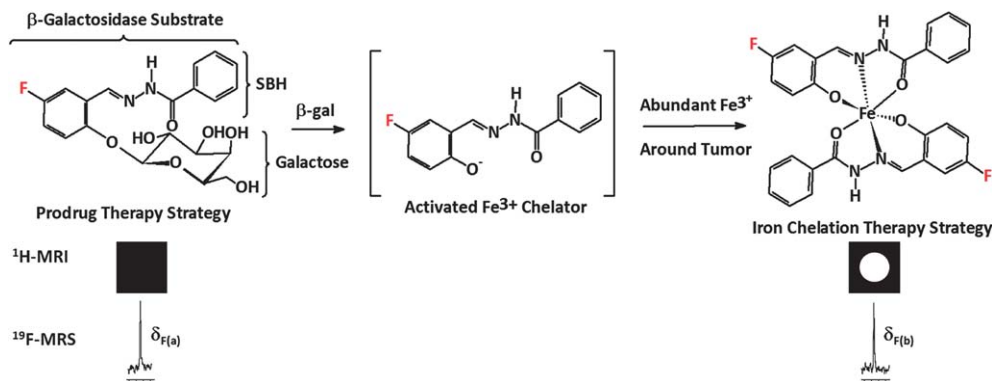


Fig. 2 Proposed mechanism of ^{19}F -MRS/ ^1H -MRI probe for detection of β -gal activity.

these ligands have the potential to maintain coordinative saturation while providing the opportunity for water to form hydrogen bonds with the catecholate oxygen atoms, which is fundamentally related to the effectiveness of the Fe^{3+} -based ^1H -MRI contrast agents.^{46–49}

For proof of principle, we started with the simple molecule 3-fluorocatechol (3-FCAT). ^{19}F -MRS of 3-FCAT in PBS gave a sharp ^{19}F -signal at $\delta_{\text{F}} = -60.80$ ppm, which showed neither changes of ^{19}F chemical shift nor ^{19}F -signal intensity upon the addition of FAC during the formation of the corresponding 3 : 1 Fe-complex $[\text{Fe}(3\text{-FCAT}\cdot 2\text{H})_3]^{3-}$ (3-FCAT/ Fe^{3+}) but a color change of the solution from clear to dark purple then black, verifying the complex formation. This result was validated by the same ^{19}F -MRS data from direct acquisition of the prepared 3-FCAT/ Fe^{3+} . Very interestingly, ^1H -MRI experiments of 3-FCAT/ Fe^{3+} clearly showed significant differences in both T_1 - and T_2 -weighted images (Fig. 6), which suggested the potential for combining T_1 and T_2 responses as concerted effects for the addition of certainty to the imaging assessment, where tissue heterogeneity may otherwise be misinterpreted. These results are consistent with our previous observations with catecholate-coumarins as Fe^{3+} -based ^1H -MRI contrast agents.^{16,48} In this situation the calculated distance from ^{19}F to paramagnetic Fe^{3+} is only $r = 4.82$ Å, which indicates that ^{19}F -atoms in bidentate 3-FCAT/ Fe^{3+} structure are not distributed within the region of Fe^{3+} anisotropic PRE interaction. These results were further confirmed by using the 3-FCAT isomer, 4-fluorocatechol (4-FCAT), with the resulting consistency through the identical tests, as shown in Fig. S2,[†] in which 4-FCAT and its Fe-complex $[\text{Fe}(4\text{-FCAT}\cdot 2\text{H})_3]^{3-}$ (4-FCAT/ Fe^{3+}) both appeared as sharp peaks at $\delta_{\text{F}} = -47.10$ ppm in PBS, accompanying substantial differences of T_1 -

and T_2 -weighted images with the distance $r = 6.53$ Å between ^{19}F and Fe^{3+} .

β -D-Galactopyranosides synthesis

Escherichia coli (*lacZ*) β -gal catalyzes the hydrolysis of β -D-galactopyranosides by cleavage of the C–O bond between D-galactose and the aglycones with overall retention of β -anomeric configuration. After the demonstration of simultaneous ^{19}F -MRS/ ^1H -MRI dual-function, β -D-galactopyranosyl group was introduced to 3- and 4-FCAT for generating their β -D-galactopyranosides in order to screen β -gal ^{19}F -MRS/ ^1H -MRI dual-function reporters.

The phenol hydroxyl pK_{a} values of 3- and 4-FCAT corresponding to their positions were calculated using the Advanced Chemistry Development Software (<http://www.acdlabs.com>) (Table 1). The noticeably lower pK_{a} of the hydroxyl group in the meta-position to the ^{19}F -atom suggested that phase-transfer-catalysis at $\text{pH} = 8$ –9 could provide regioselective synthesis of mono- β -D-galactopyranosides, as we exploited previously for β -gal ^{19}F -MRS/MRI reporters.^{19,20,25,48} Reaction of 2,3,4,6-tetra-*O*-acetyl- α -D-galactopyranosyl bromide with an equimolar amount of 3- or 4-FCAT at room temperature catalyzed by tetrabutylammonium bromide (TBAB) in a dichloromethane-aqueous biphasic system ($\text{pH} = 8$ –9) under N_2 atmosphere afforded 1-*O*-(2',3',4',6'-tetra-*O*-acetyl- β -D-galactopyranosyl)-3-fluorocatechol (MG-3-FCAT) (95%) and 2-*O*-(2',3',4',6'-tetra-*O*-acetyl- β -D-galactopyranosyl)-4-fluorocatechol (MG-4-FCAT) (88%), respectively (Fig. 7). NOESY spectra displaying the correlations between anomeric H-1' and H-6 in MG-3-FCAT or H-3 in MG-4-FCAT showed the mono- β -D-galactopyranosylations occurred at

| Complex | PIH/ Fe^{3+} | SBH/ Fe^{3+} | SIH/ Fe^{3+} | SNH/ Fe^{3+} |
|---|-----------------------|-----------------------|-----------------------|-----------------------|
| T_1 -weighted ^1H -MRI (Control) | | | | |
| T_1 -weighted ^1H -MRI (Complex) | | | | |

Fig. 3 The comparison of ^1H -MRI effect of the Fe-complexes from ligands PIH, SBH, SIH and SNH with ferric ammonium citrate (FAC). (A) Control, FAC (8 mM) in 1 : 1 (v/v) DMSO/PBS (0.1 M, $\text{pH} = 7.4$); (B) complex, PIH, SBH, SIH or SNH each (16 mM), FAC (8 mM) in 1 : 1 (v/v) DMSO/PBS (0.1 M, $\text{pH} = 7.4$); conditions: T_1 -weighted ^1H -MRI, 200 MHz, $\text{TR} = 300$ ms, $\text{TE} = 20$ ms, 1.5 mm slice, 128×128 , $50 \text{ mm} \times 50 \text{ mm}$.

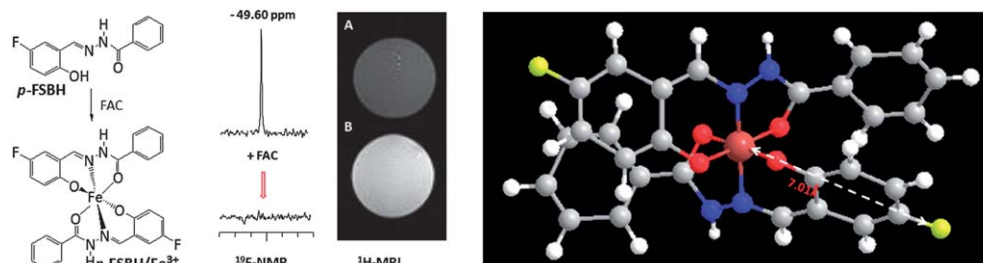


Fig. 4 The ^{19}F -MRS/ ^1H -MRI and molecular characterization of **p-FSBH** to **p-FSBH/Fe $^{3+}$** . ^{19}F -MRS: (1) **p-FSBH** (1.3 mg, 5.0 μmol) in 1 : 1 (v/v) DMSO/PBS (0.1 M, pH = 7.4, 600 μL) at 25 $^\circ\text{C}$; (2) **p-FSBH** (1.3 mg, 5.0 μmol) in 1 : 1 (v/v) DMSO/PBS (0.1 M, pH = 7.4, 500 μL), FAC (663 μg , 2.5 μmol) in PBS (0.1 M, pH = 7.4, 100 μL) at 25 $^\circ\text{C}$, ^{19}F -NMR parameter sets: relaxation delay: 1 s, pulse width (90°): 16.6 μs , number of points acquired: 59 966, filter bandwidth: 28 000 Hz, each spectrum acquisition time: 0.6 s, number of acquisitions: 128, and enhanced with an exponential line broadening of 40 Hz. ^1H -MRI: (A) control, **p-FSBH** (10.0 mM) in 1 : 1 (v/v) DMSO/PBS (0.1 M, pH = 7.4) at 20–22 $^\circ\text{C}$; (B) complex, **p-FSBH** (10.0 mM), FAC (5.0 mM) in 1 : 1 (v/v) DMSO/PBS (0.1 M, pH = 7.4) at 20–22 $^\circ\text{C}$; conditions: T_1 -weighted ^1H -MRI: using the same parameters as in Fig. 3; molecular modelling calculation: the minimized energy conformation of **p-FSBH/Fe $^{3+}$** was obtained by the molecular calculation program Chem3D 8.0, using MM2 as the force-field, and the distance of F- to paramagnetic Fe^{3+} $r = 7.01 \text{ \AA}$ was calculated by using Visual Molecular Dynamics (VMD 1.9), white balls: H atoms, grey balls: C atoms, red balls: O atoms, blue balls: N atoms, yellow balls: F atoms, dark red ball: Fe atom.

the hydroxyl group in meta-position to the ^{19}F -atom, as predicted. Subsequent deacetylation with NH_3/MeOH from 0 $^\circ\text{C}$ to room temperature gave the free mono-galactopyranosides **MGD-3-FCAT** and **MGD-4-FCAT** in nearly quantitative yields. The anomeric β -D-configuration of **MGD-3-FCAT** and **MGD-4-FCAT** in the $^4\text{C}_1$ chair conformation was confirmed by the ^1H -NMR chemical shifts $\delta_{\text{H}-1'}$ = 4.62–4.67 ppm of the anomeric protons, and the coupling constants of $J_{1',2'}$ = 8 Hz and $J_{2',3'}$ = 10 Hz. The anomeric carbon resonances appeared at $\delta_{\text{C}-1'}$ 102.68–105.75 ppm are in accordance with the β -D-configuration.^{19,20}

Molecular MRI of intracellular targets and processes must rely on the effective uptake of contrast agents by cells *in vivo*, requiring sufficient solubility and the capability to enter cells. As demonstrated in clinical applications, carbohydrate-associated prodrugs showed improved water solubility and permeability, leading to better selectivity and efficacy of chemotherapy.⁵⁰ Accordingly, we sought to conjugate an additional β -D-galactopyranosyl unit to **MGD-3-FCAT** and **MGD-4-FCAT**. Condensation of 3- or 4-FCAT directly with 2.2 equivalents of 2,3,4,6-tetra-O-acetyl- α -D-galactopyranosyl bromide in anhydrous $\text{CH}_2\text{Cl}_2/\text{MeCN}$ catalyzed by $\text{Hg}(\text{CN})_2$ as a promoter,

furnished the fully galactopyranosylated fluorocatechols: 1,2-di-O-(2',3',4',6'-tetra-O-acetyl- β -D-galactopyranosyl)-3-fluorocatechol (**FG-3-FCAT**) (93%) and 1,2-di-O-(2',3',4',6'-tetra-O-acetyl- β -D-galactopyranosyl)-4-fluorocatechol (**FG-4-FCAT**) (86%), respectively (Fig. 7). Deacetylation of **FG-3-FCAT** and **FG-4-FCAT** in NH_3/MeOH from 0 $^\circ\text{C}$ to room temperature accomplished the free di- β -D-galactopyranosides **FGD-3-FCAT** and **FGD-4-FCAT** in high yields. The ESI-MS of **FGD-3-FCAT** and **FGD-4-FCAT** displayed the expected molecular ions, corresponding to the fully galactopyranosylated derivatives. The structures of **FGD-3-FCAT** and **FGD-4-FCAT** were confirmed by their ^1H and ^{13}C -NMR spectra. The anomeric protons H-1', H-1'' of D-galactoses linked to 1,2-positions of fluorocatechols 3- and 4-FCAT at 4.53–4.83 ppm with the well resolved doublets ($J_{1',2'} = J_{1'',2''} = 8 \text{ Hz}$, $J_{2',3'} = J_{2'',3''} = 10 \text{ Hz}$) confirmed both D-galactoses in the β -configuration. As expected, di- β -D-galactopyranosides **FGD-3-FCAT** and **FGD-4-FCAT** are soluble in PBS (0.1 M, pH = 7.4) in high concentrations (**FGD-3-FCAT**: 402 mg mL^{-1} and **FGD-4-FCAT**: 337 mg mL^{-1} in PBS at room temperature), unlike **MGD-3-FCAT** and **MGD-4-FCAT**, which required the addition of DMSO for such high concentrations, as previously successfully applied to β -gal ^{19}F -NMR and ^1H -MRI reporters.^{20,48}

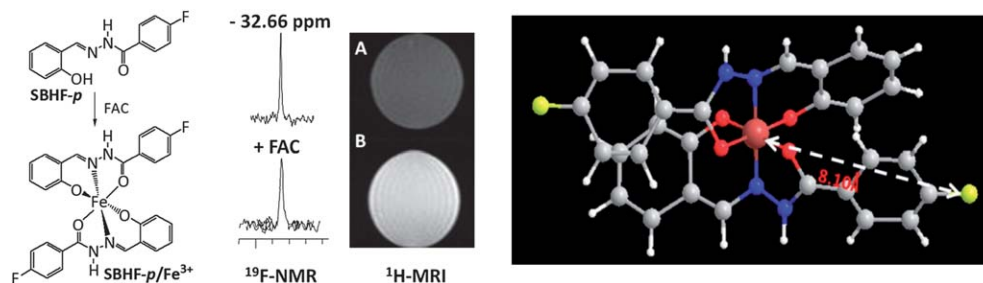


Fig. 5 The ^{19}F -MRS/ ^1H -MRI and molecular characterization of **SBHF-p** to **SBHF-p/Fe $^{3+}$** . ^{19}F -MRS: (1) **SBHF-p** (1.2 mg, 4.5 μmol) in 1 : 1 (v/v) DMSO/PBS (0.1 M, pH = 7.4, 600 μL) at 25 $^\circ\text{C}$; (2) **SBHF-p** (1.2 mg, 4.5 μmol) in 1 : 1 (v/v) DMSO/PBS (0.1 M, pH = 7.4, 500 μL), FAC (596 μg , 2.3 μmol) in PBS (0.1 M, pH = 7.4, 100 μL) at 25 $^\circ\text{C}$, ^{19}F -NMR: using the same parameters as in Fig. 4. ^1H -MRI: (A) control, **SBHF-p** (9.0 mM) in 1 : 1 (v/v) DMSO/PBS (0.1 M, pH = 7.4) at 20–22 $^\circ\text{C}$; (B) complex, **SBHF-p** (9.0 mM), FAC (4.5 mM) in 1 : 1 (v/v) DMSO/PBS (0.1 M, pH = 7.4) at 20–22 $^\circ\text{C}$; conditions: T_1 -weighted ^1H -MRI: using the same parameters as in Fig. 3; molecular modelling calculation: using the same programs as in Fig. 4, $r = 8.10 \text{ \AA}$.

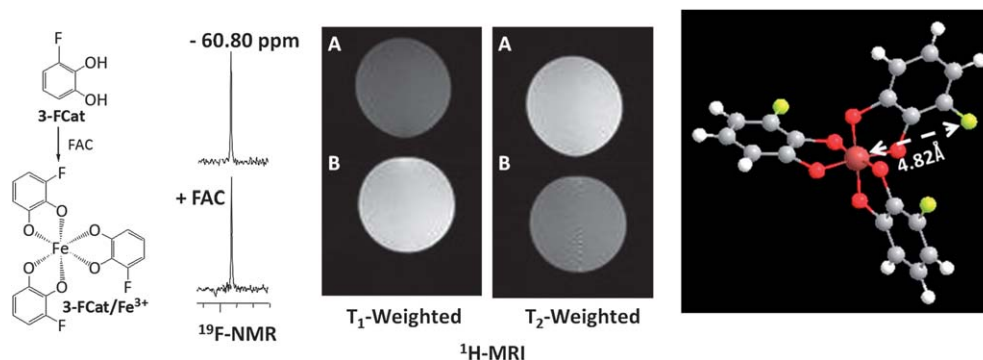


Fig. 6 The ^{19}F -MRS/ ^1H -MRI and molecular characterization of **3-FCAT** to **3-FCAT/Fe $^{3+}$** . ^{19}F -MRS: (1) **3-FCAT** (1.2 mg, 9.0 μmol) in PBS (0.1 M, pH = 7.4, 600 μL) at 25 $^\circ\text{C}$; (2) **3-FCAT** (1.2 mg, 9.0 μmol) in PBS (0.1 M, pH = 7.4, 500 μL), FAC (796 μg , 3.0 μmol) in PBS (0.1 M, pH = 7.4, 100 μL) at 25 $^\circ\text{C}$, ^{19}F -NMR: using the same parameters as in Fig. 4. ^1H -MRI: (A) control, **3-FCAT** (12.0 mM) in PBS (0.1 M, pH = 7.4) at 20–22 $^\circ\text{C}$; (B) complex, **3-FCAT** (12.0 mM), FAC (4.0 mM) in PBS (0.1 M, pH = 7.4) at 20–22 $^\circ\text{C}$; conditions: T_1 -weighted ^1H -MRI: using the same parameters as in Fig. 3; T_2 -weighted ^1H -MRI: 200 MHz, TR = 2000 ms, TE = 80 ms, 1.5 mm slice, 128 \times 128, 50 mm \times 50 mm; molecular modelling calculation: using the same programs as in Fig. 4, $r = 4.82$ \AA .

Table 1 The hydroxyl pK_a values of 3- and 4-fluorocatechols

| Fluorocatechols | $\text{pK}_{a(\text{OH}-1)}$ | $\text{pK}_{a(\text{OH}-2)}$ |
|------------------------------------|------------------------------|------------------------------|
| 3-Fluorocatechol (3-FCAT) | 8.54 ± 0.10 | 11.54 ± 0.10 |
| 4-Fluorocatechol (4-FCAT) | 12.55 ± 0.18 | 8.80 ± 0.10 |

β -Gal hydrolysis

Kinetic ^{19}F -MRS were applied to analyze the reactions of β -gal with mono-galactopyranosides **MGD-3-FCAT**, **MGD-4-FCAT** and di- β -D-galactopyranosides **FGD-3-FCAT**, **FGD-4-FCAT**.^{18–25} **MGD-3-FCAT**, **MGD-4-FCAT** and **FGD-3-FCAT**, **FGD-4-FCAT** in PBS (0.1 M, pH = 7.4) each gave a narrow ^{19}F -signal at $\delta_{\text{F}} = -54.55$, -46.29 , -52.85 and -43.13 ppm, respectively. Following the reaction with β -gal (E801A) in PBS (0.1 M, pH = 7.4) at 37 $^\circ\text{C}$, the kinetic ^{19}F -MRS measurement of ^{19}F chemical shift and signal intensity changes at each time point (0–60 min) indicated that **MGD-3-FCAT**, **FGD-3-FCAT** converted to **3-FCAT** ($\delta_{\text{F}} = -60.80$ ppm), and **MGD-4-FCAT**, **FGD-4-FCAT** to **4-FCAT** ($\delta_{\text{F}} = -47.10$ ppm) with various hydrolytic rates (Table 2 and Fig. 8). Fig. 9 showed the ^{19}F -MRS time course spectra of **MGD-3-FCAT** with β -gal (E801A) in PBS (0.1 M, pH = 7.4) at 37 $^\circ\text{C}$. The hydrolysis of **MGD-3-FCAT**, **FGD-3-FCAT** and **MGD-4-FCAT**, **FGD-4-FCAT** proceeded smoothly, indicating that these four substrates and the liberated **3-FCAT** and **4-FCAT** had no inhibitory effects on β -

Table 2 ^{19}F -MRS chemical shifts (ppm) and hydrolytic rates ($\mu\text{M min}^{-1}$ per unit) of **MGD-3-FCAT**, **MGD-4-FCAT** and **FGD-3-FCAT**, **FGD-4-FCAT** with β -gal (5 units, E801A) in PBS (0.1 M, pH = 7.4, 600 μL) at 37 $^\circ\text{C}$

| No. | MGD-3-FCAT | MGD-4-FCAT | FGD-3-FCAT | FGD-4-FCAT |
|---------------------------------------|-------------------|-------------------|-------------------|-------------------|
| $\delta_{\text{F}}(\text{substrate})$ | -54.55 | -46.29 | -52.85 | -43.13 |
| $\delta_{\text{F}}(\text{aglycone})$ | -60.80 | -47.10 | -60.80 | -47.10 |
| $\Delta\delta$ | 6.25 | 0.81 | 7.95 | 3.97 |
| ν | 328.57 | 283.93 | 10.51 | 38.33 |

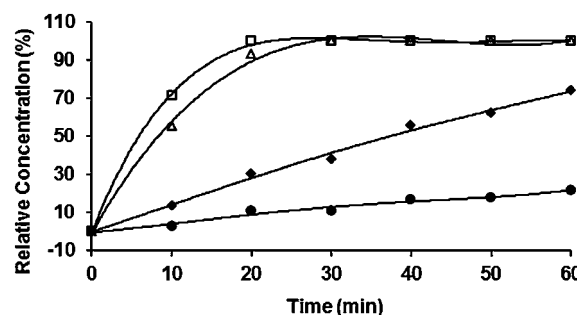


Fig. 8 The kinetic hydrolysis time courses of mono- β -D-galactopyranosides **MGD-3-FCAT** \rightarrow **3-FCAT** (\square), **MGD-4-FCAT** \rightarrow **4-FCAT** (Δ), and di- β -D-galactopyranosides **FGD-3-FCAT** \rightarrow **3-FCAT** (\bullet), **FGD-4-FCAT** \rightarrow **4-FCAT** (\blacklozenge) (23.0 mM each) with β -gal (5 units, E801A) in PBS (0.1 M, pH = 7.4, 600 μL) at 37 $^\circ\text{C}$.

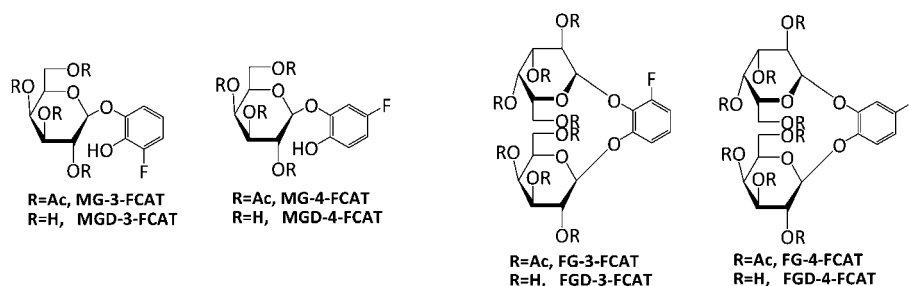


Fig. 7 The structures of mono- β -D-galactopyranosides **MG-3-FCAT**, **MG-4-FCAT**, **MGD-3-FCAT**, **MGD-4-FCAT**, and di- β -D-galactopyranosides **FG-3-FCAT**, **FG-4-FCAT**, **FGD-3-FCAT**, **FGD-4-FCAT**.

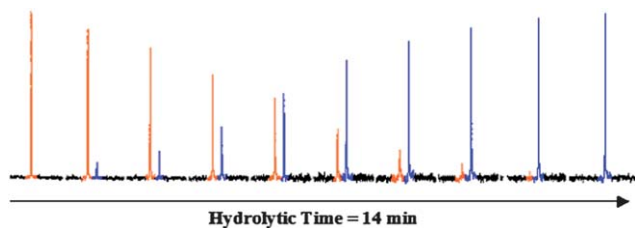


Fig. 9 ^{19}F -MRS spectra of time course. Mono- β -D-galactopyranoside **MGD-3-FCAT** (4.0 mg, 13.8 μmol), β -gal (5 units, E801A) in PBS (0.1 M, pH = 7.4, 600 μL) at 37 $^{\circ}\text{C}$, ^{19}F -MRS: using the same parameters as in Fig. 4, number of acquisitions: 64, pre-acquisition delay: 0 s, red peaks: **MGD-3-FCAT** at $\delta_{\text{F}} = -54.55$ ppm, blue peaks: **3-FCAT** at $\delta_{\text{F}} = -60.80$ ppm.

gal (E801A). Given that **MGD-3-FCAT** and **MGD-4-FCAT** both were much more reactive substrates to β -gal, **MGD-3-FCAT** also showed larger ^{19}F chemical shift change ($\Delta\delta_{\text{F}} = 6.25$ ppm), making it favored for the further evaluation. To verify the specificity, **MGD-3-FCAT** was incubated with other similar enzymes α -galactosidase (Sigma G7163) and β -glucuronidase (Sigma G8295) in PBS (0.1 M, pH = 7.4) at 37 $^{\circ}\text{C}$, however, **MGD-3-FCAT** showed the resistance to both, and maintained its ^{19}F -signal at $\delta_{\text{F}} = -54.55$ ppm over the period of 60 min.

^{19}F -MRS/ ^1H -MRI dual detection of β -gal activity in solution

Having a β -gal ^{19}F -MRS/ ^1H -MRI substrate in hand, we moved on to the detection of β -gal activity using ^{19}F -MRS/ ^1H -MRI dual-function. ^{19}F -MRS of the mixture of **MGD-3-FCAT** and

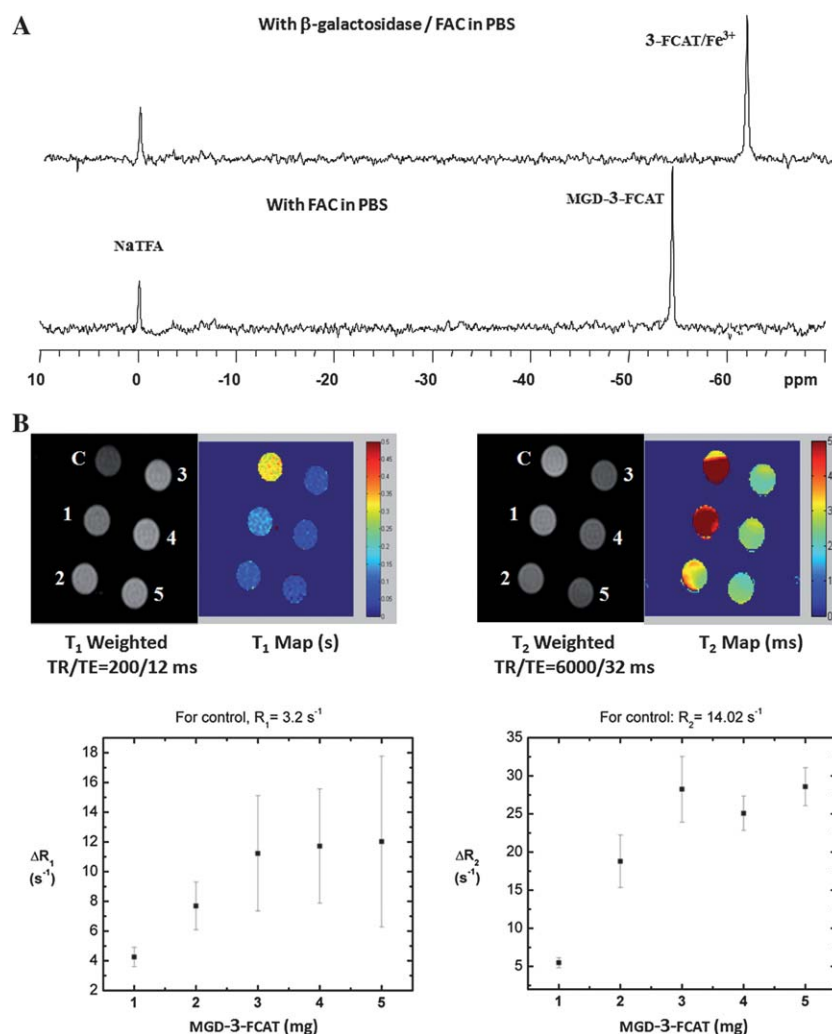


Fig. 10 (A) ^{19}F -MRS detection of β -gal activity. **MGD-3-FCAT** (4.0 mg, 13.8 μmol), FAC (1.2 mg, 4.5 μmol), without and with β -gal (5 units, E801A) in PBS (0.1 M, pH = 7.4, 600 μL) at 37 $^{\circ}\text{C}$, ^{19}F -MRS: using the same parameters as in Fig. 4, number of acquisitions: 64, **MGD-3-FCAT** at $\delta_{\text{F}} = -54.55$ ppm, **3-FCAT/Fe $^{3+}$** at $\delta_{\text{F}} = -60.80$ ppm. (B) ^1H -MRI detection of β -gal activity. Conditions: ^1H -MRI, 200 MHz, 1 mm slice, 128 \times 256, 32 mm \times 64 mm. (C) Control, **MGD-3-FCAT** (3.0 mg, 10.3 μmol), FAC (10.0 μmol), without β -gal (E801A), TFA (2.0 μmol), PBS (1.5 mL); (1) **MGD-3-FCAT** (1.0 mg, 3.5 μmol), FAC (10.0 μmol), β -gal (E801A, 5 units), TFA (2.0 μmol), PBS (1.5 mL); (2) **MGD-3-FCAT** (2.0 mg, 6.9 μmol), FAC (10.0 μmol), β -gal (E801A, 5 units), TFA (2.0 μmol), PBS (1.5 mL); (3) **MGD-3-FCAT** (3.0 mg, 10.3 μmol), FAC (10.0 μmol), β -gal (E801A, 5 units), TFA (2.0 μmol), PBS (1.5 mL); (4) **MGD-3-FCAT** (4.0 mg, 13.8 μmol), FAC (10.0 μmol), β -gal (E801A, 5 units), TFA (2.0 μmol), PBS (1.5 mL); (5) **MGD-3-FCAT** (5.0 mg, 17.2 μmol), FAC (10.0 μmol), β -gal (E801A, 5 units), TFA (2.0 μmol), PBS (1.5 mL) at 37 $^{\circ}\text{C}$ in 30 min. For FAC (10.0 μmol) alone in PBS (0.1 M, pH = 7.4, 1.5 mL), $R_1 = 3.0$ s $^{-1}$, $R_2 = 11.1$ s $^{-1}$.

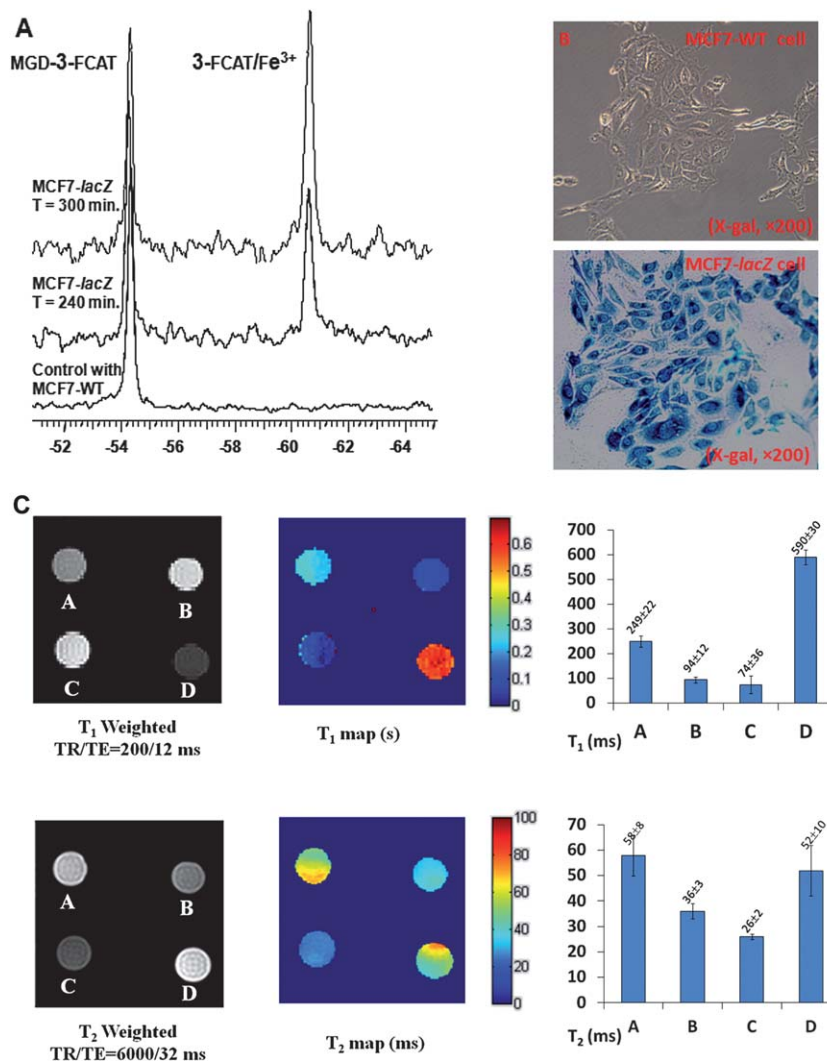


Fig. 11 (A) *In vitro* ¹⁹F-MRS detection of *lacZ* gene expression in MCF7-*lacZ* cells. (1) Control: **MGD-3-FCAT** (2.6 mg, 9.0 μmol), FAC (797.4 μg, 3.0 μmol), with MCF7-WT cells (5 × 10⁶) in PBS (0.1 M, pH = 7.4, 600 μL) at 37 °C; (2) **MGD-3-FCAT** (2.6 mg, 9.0 μmol), FAC (797.4 μg, 3.0 μmol), with MCF7-*lacZ* cells (5 × 10⁶) in PBS (0.1 M, pH = 7.4, 600 μL) at 37 °C at different time points, *t* = 240 and 300 minutes, ¹⁹F-MRS: using the same parameters as in Fig. 9, **MGD-3-FCAT** at δ_F = -54.55 ppm, **3-FCAT/Fe³⁺** at δ_F = -60.80 ppm. (B) β-gal activity validation in MCF7-*lacZ* cells with deep blue (bottom) and no activity in MCF7-WT cells (top), X-gal staining (200×). (C) *In vitro* ¹H-MRI detection of *lacZ* gene expression in MCF7-*lacZ* cells after 25 hour incubation at 37 °C. Conditions: ¹H-MRI, 200 MHz, 1 mm slice, 128 × 128, 25.6 mm × 25.6 mm. (A) Control, **MGD-3-FCAT** (3.0 mg, 10.3 μmol), FAC (5.0 μmol), TFA (2.0 μmol), MCF7-WT cells (5 × 10⁶) in PBS (0.1 M, pH = 7.4, 850 μL); (B) **MGD-3-FCAT** (3.0 mg, 10.3 μmol), FAC (5.0 μmol), TFA (2.0 μmol), MCF7-*lacZ* cells (5 × 10⁶) in PBS (0.1 M, pH = 7.4, 850 μL); (C) **MGD-3-FCAT** (5.8 mg, 20.0 μmol), FAC (5.0 μmol), TFA (2.0 μmol), MCF7-*lacZ* cells (5 × 10⁶) in PBS (0.1 M, pH = 7.4, 850 μL); (D) **MGD-3-FCAT** (3.0 mg, 10.3 μmol), without FAC, TFA (2.0 μmol), MCF7-*lacZ* cells (5 × 10⁶) in PBS (0.1 M, pH = 7.4, 850 μL).

FAC in PBS (0.1 M, pH = 7.4) displayed a sharp ¹⁹F-signal at δ_F = -54.55 ppm. Upon the addition of β-gal (E801A) as the reaction proceeded at 37 °C, the appearance of a new single ¹⁹F-peak of **3-FCAT/Fe³⁺** was observed in a time-dependent manner at δ_F = -60.80 ppm (Fig. 10A). The formation of the **3-FCAT/Fe³⁺** complex during the enzymatic reaction of **MGD-3-FCAT** in the presence of FAC was confirmed by LC/MS(ESI⁺) data, in which the substrate **MGD-3-FCAT** and complex **3-FCAT/Fe³⁺** were detected in HPLC chromatograms at 4.4 and 16.1 min, corresponding to *m/z* 313.9 [M + Na]⁺ of **MGD-3-FCAT** (calculated *m/z* 313.2), and *m/z* 437.8 [M]⁺ of [Fe(3-FCAT-H)₃] (calculated *m/z* 437.1), respectively. The relaxation times T₁ and T₂ were measured for vials containing various amounts

of **MGD-3-FCAT** (3.5–17.2 μmol) and a fixed concentration of FAC (10.0 μmol), without or with β-gal (E801A, 5 units). Addition of β-gal to the mixture solution of **MGD-3-FCAT** and FAC at 37 °C for 30 min generated greater relaxation rate differences ΔR₁ and ΔR₂ (Fig. 10B), which are increasingly associated with the accumulation of Fe-complex **3-FCAT/Fe³⁺** formed *in situ* (Fig. S3[†]). By the comparison with the relaxation rates R₁ = 3.0 and R₂ = 11.1 s⁻¹ of FAC solution, we found that the interaction of β-D-galactopyranoside **MGD-3-FCAT** and Fe³⁺ (R₁ = 3.2 and R₂ = 14.0 s⁻¹, Fig. 10B) also produced small relaxivity, which suggested that the weaker complexity of carbohydrate with trivalent Fe³⁺ (ref. 51) results in the increase of nonlinear ΔR.

¹⁹F-MRS/¹H-MRI simultaneous assessments of *lacZ* gene expression in transfected cancer cells

In order to demonstrate the potential for *in vivo* application, ¹⁹F-MRS/¹H-MRI dual functional detections of *lacZ* gene expression in human MCF7 breast and PC3 prostate cancer cells were confirmed. The cytotoxicity of **MGD-3-FCAT** was examined for both the conjugate and the cleavage product using both wild-type and *lacZ* expressing MCF7 and PC3 cells (Fig. S4†). Because of releasing acute toxic **3-FCAT** (Category 4, GHS Classification) in MCF7- and PC3-*lacZ* cells, Fig. S4† showed that **MGD-3-FCAT** is more toxic in these β-gal expressing cells. After incubation of **MGD-3-FCAT** with wild type (WT) and *lacZ* transfected human MCF7 breast cancer cells in the presence of FAC in PBS (0.1 M, pH = 7.4) at 37 °C under 5% CO₂ in air with 95% humidity, the mixtures were subjected to ¹⁹F-MRS analysis at different time points. At the starting point (0 min), **MGD-3-FCAT** in MCF7-WT/FAC or MCF7-*lacZ*/FAC both exhibited a single narrow ¹⁹F-signal at δ_F = -54.55 ppm. As the time of incubation went on, the ¹⁹F-peak of **MGD-3-FCAT** in MCF7-WT/FAC remained unchanged. But in MCF7-*lacZ*/FAC cell solution, a new single ¹⁹F-peak of **3-FCAT/Fe³⁺** at δ_F = -60.80 ppm was seen and progressively grown in a smooth monotonic manner with the rate of ν = 5.48 μM min⁻¹ per million cells (Fig. 11A), whereas the rate was 1.90 times higher when incubated with equal numbers of lysed MCF7-*lacZ* cells. The β-gal activity in MCF7-*lacZ* cells was validated by X-gal staining, which turned to deep blue, whereas MCF7-WT cells showed no blue color (Fig. 11B). Significant differences in relaxation times *T*₁ and *T*₂ were observed between the *lacZ* transfected and WT MCF7 breast cancer cells after incubation for 25 hours. In MCF7-WT cells relaxation rates were determined to be *T*₁ = 249 ± 22 ms and *T*₂ = 58 ± 8 ms, while in MCF7-*lacZ* cells *T*₁ = 94 ± 12 ms and *T*₂ = 36 ± 3 ms were observed [compared with the same concentration of **MGD-3-FCAT** (12.12 mM), the *T*₁ and *T*₂ values with various concentrations are represented as bars at the right sides adjacent to *T*₁ and *T*₂ maps] (Fig. 11C).

In similarly incubated intact PC3-*lacZ* cells, the rate of conversion from **MGD-3-FCAT** (δ_F = -54.55 ppm) to **3-FCAT** (δ_F = -60.80 ppm) is ν = 862.86 μM min⁻¹ per million cells, and 1.86 times higher with the same numbers of lysed PC3-*lacZ* cells. These differences between intact and lysed cells indicate that membrane permeation is a big obstruction to β-gal reaction in MCF7- and PC3-*lacZ* cells. The relaxation times were *T*₁ = 466 ± 62 ms and *T*₂ = 143 ± 4 ms in PC3-WT cells, whereas for PC3-*lacZ* cells *T*₁ = 204 ± 60 ms and *T*₂ = 101 ± 3 ms after 25 hour incubation were obtained [with **MGD-3-FCAT** (15.13 mM)], respectively (Fig. S5†).

Conclusion

In summary, we present here a novel bimodal approach of synergizing ¹⁹F-MRS/¹H-MRI for the detection of β-gal activity, in which ¹⁹F-MRS is used to define β-gal responsive ¹⁹F-chemical shift changes and hydrolytic kinetics for identification of the presence and progression of β-gal. Concurrently, ¹H-MRI

shows the location and magnitude of β-gal. Both signals are simultaneously generated and enhanced in the “turn-on” mode from the same site and identity, resulting in better assessing precision and reliability.

Along with this bimodal reporter design, we have successfully synthesized and characterized a series of ¹⁹F-MRS/¹H-MRI probes, and demonstrated the feasibility of **MGD-3-FCAT** assessing β-gal activity in solution and *in vitro* with *lacZ* transfected tumor cells in the presence of Fe³⁺ ions. ¹⁹F-MRS/¹H-MRI clearly revealed WT *versus lacZ*-transfected cells in culture upon incubation with **MGD-3-FCAT** based on the significant differences in ¹⁹F-chemical shift change and both *T*₁ and *T*₂, in which the concerted responses for adding certainty show most promising for validation of β-gal detection. We demonstrate the first example using anisotropic Fe³⁺-¹⁹F PRE effect to assay β-gal activity by real-time ¹⁹F-MRS/¹H-MRI.

In the present studies, we introduced exogenous Fe³⁺, ultimately, we hope to develop this approach to scavenge the elevated Fe³⁺ of tumors for ¹H-MRI signal generation. Indeed, aroyl hydrazones and catechols are in clinical use as Fe³⁺ scavenging agents suggesting a potential for clinical theranostic application.

Experimental

General methods

NMR spectra were recorded on a Varian Unity INOVA 400 spectrometer (400 MHz for ¹H, 100 MHz for ¹³C, 376 MHz for ¹⁹F), ¹H and ¹³C chemical shifts are referenced to TMS as the internal standard with CDCl₃, or DMSO-d₆ as solvents. ¹⁹F uses a dilute solution of NaTFA in a capillary as the external standard, chemical shifts are given in ppm. All compounds were characterized by NMR at 25 °C. Microanalyses were performed on a Perkin-Elmer 2400CHN microanalyser. Mass spectra were obtained by positive and negative ESI-MS using a Micromass Q-TOF hybrid quadrupole/time-of-flight instrument (Micromass UK Ltd). LC/MS data were obtained using a HP Agilent 1100 Series LC/MSD on an Eclipse XDB-C18 column with 70%/30% CH₃CN/H₂O as eluents.

Solutions in organic solvents were dried with anhydrous sodium sulfate, and concentrated *in vacuo* below 45 °C. 2,3,4,6-Tetra-*O*-acetyl-α-D-galactopyranosyl bromide was purchased from the Sigma Chemical Company. β-Gal (E801A) was purchased from Promega (Madison, WI, USA) and enzymatic reactions were performed at 37 °C in PBS solution (0.1 M, pH = 7.4). Column chromatography was performed on silica gel (200–300 mesh) and silica gel GF₂₅₄ used for analytical TLC was purchased from the Aldrich Chemical Company. Detection was effected by spraying the plates with 5% ethanolic H₂SO₄ (followed by heating at 110 °C for 10 min) or by direct UV illumination of the plate. The purity of the final products was determined by HPLC with ≥95%.

Mono-β-D-galactopyranosides MG-3-FCAT and MG-4-FCAT

General procedure – a solution of 2,3,4,6-tetra-*O*-acetyl-α-D-galactopyranosyl bromide (1.62 g, 3.93 mmol) in CH₂Cl₂

(50 mL) was added dropwise to a vigorously stirred biphasic mixture (pH 8–9) of 3- or 4-fluorocatechol (0.50 g, 3.93 mmol) and tetrabutylammonium bromide (TBAB) (160 mg, 0.5 mmol) in CH_2Cl_2 - H_2O (80 mL, 1 : 1 v/v') over a period of 1 h at room temperature under an N_2 atmosphere, and the stirring continued for additional ~ 3 h until TLC showed that the reaction was completed. The products were extracted with CH_2Cl_2 (4×30 mL), washed (H_2O), dried (Na_2SO_4), and evaporated under reduced pressure to give a syrup, which was purified by column chromatography on silica gel to give the acetylated mono- β -D-galactopyranosides **MG-3-FCAT** and **MG-4-FCAT**.

Di- β -D-galactopyranosides **FG-3-FCAT** and **FG-4-FCAT**

General procedure – to a vigorously stirred solution of 3- and 4-fluorocatechols (0.32 g, 2.50 mmol) and $\text{Hg}(\text{CN})_2$ (2.10 g, 8.25 mmol) in anhydrous MeCN (80 mL) containing freshly activated 4 Å molecular sieves (5.0 g) was added dropwise 2,3,4,6-tetra-*O*-acetyl- α -D-galactopyranosyl bromide (2.26 g, 5.50 mmol, 2.2 equiv.) in CH_2Cl_2 (50 mL). The mixture was stirred continually in the dark at room temperature under N_2 atmosphere until TLC indicated that the reaction was completed, then diluted with CH_2Cl_2 (100 mL), filtered through Celite, washed, dried (Na_2SO_4), and evaporated under reduced pressure to give a syrup, which was purified by column chromatography on silica gel to give the acetylated di- β -D-galactopyranosides **FG-3-FCAT** and **FG-4-FCAT**.

Free mono- and di- β -D-galactopyranosides **MGD-3-FCAT**, **MGD-4-FCAT**, **FGD-3-FCAT** and **FGD-4-FCAT**

General procedure – a solution of acetylated mono- β -D-galactopyranosides **MG-3-FCAT** or **MG-4-FCAT** (950 mg), or di-*O*-(2',3',4',6'-tetra-*O*-acetyl- β -D-galactopyranosyl) fluorocatechols **FG-3-FCAT** or **FG-4-FCAT** (1.50 g) in anhydrous MeOH (100 mL) containing 0.5 M NH_3 was vigorously stirred from 0 °C to room temperature overnight until TLC showed that the reaction was completed, and evaporated to dryness *in vacuo*. Chromatography of the crude syrup on silica gel with ethyl acetate-methanol (1 : 2, 1 : 4) afforded the corresponding free mono- β -D-galactopyranosides **MGD-3-FCAT**, **MGD-4-FCAT** and di- β -D-galactopyranosides **FGD-3-FCAT**, **FGD-4-FCAT** in high yields.

Stable *lacZ* transfected cancer cells

E. coli lacZ gene (from pSV- β -gal vector, Promega, Madison, WI, USA) was inserted into high expression human cytomegalovirus (CMV) immediate-early enhancer/promoter vector phCMV (Gene Therapy Systems, San Diego, CA, USA) giving a recombinant vector phCMV/*lacZ*. This was used to transfect wild type MCF7 (human breast cancer) and PC3 (human prostate cancer) cells (ATCC, Manassas, VA, USA) using GenePORTER2 (Gene Therapy Systems, Genlantis, Inc., San Diego, CA, USA), as described in detail previously.^{21,22} The highest β -gal expressing colony was selected using the antibiotic G418 disulfate (800 $\mu\text{g mL}^{-1}$, Research Products International Corp, Mt Prospect, IL, USA) and G418 (200 $\mu\text{g mL}^{-1}$) was also

included for routine culture. The cells were maintained in Dulbecco's modified Eagle's medium (DMEM, Mediatech Inc., Herndon, VA, USA) containing 10% fetal bovine serum (FBS, Atlanta Biologicals, Inc., Lawrenceville, GA, USA) with 100 units mL^{-1} penicillin, 100 units mL^{-1} streptomycin, and cultured in a humidified 5% CO_2 incubator at 37 °C. The β -gal activity of *lacZ*-transfected tumor cells was measured using a β -gal assay kit with *o*-nitrophenyl- β -D-galactopyranoside (Promega, Madison, WI, USA), and confirmed by X-gal staining.^{21,22} Cell lysis was achieved by a freeze/thaw method: equal numbers of MCF7-*lacZ* or PC3-*lacZ* cells were suspended in PBS and then frozen at -80 °C for 10 min before thawing at room temperature over 3 cycles.

Cytotoxicity

The cytotoxicity of **MGD-3-FCAT** was assessed for both conjugate and the cleavage product in both wild-type and *lacZ* expressing MCF7 and PC3 cells using a colorimetric CellTiter 96 Aqueous Nonradioactive MTS Cell Proliferation Assay (Promega). Assays were performed in triplicate using 24-well plates seeded with 10^3 cells per well in 500 μL of RPMI-1640 without phenol red and supplemented with 10% FCS and 2 mM glutamine.¹⁹

Kinetic ^{19}F -MRS experiments

Relative substrate efficacy of mono-galactopyranosides **MGD-3-FCAT**, **MGD-4-FCAT** and di-galactopyranosides **FGD-3-FCAT**, **FGD-4-FCAT** was evaluated using ^{19}F -MRS. Enzyme reactions were conducted at 37 °C in PBS (0.1 M, pH = 7.4) using β -gal (E801A, Promega, Madison, WI, USA). **MGD-3-FCAT**, **MGD-4-FCAT** and **FGD-3-FCAT**, **FGD-4-FCAT** (13.8 μmol) were dissolved in PBS (595 μL , pH = 7.4) and β -gal (E801A, 5 μL , 1 unit μL^{-1}) added, followed by immediate ^{19}F -MRS data acquisition at 37 °C with subsequent spectra every 102 s providing a kinetic curve over 60 min.

MRI

MRI studies were performed using a 4.7 T horizontal bore magnet equipped with a Varian INOVA Unity system (Palo Alto, CA, USA), T_1 and T_2 maps were acquired using a spin-echo sequence with varying repetition times (TR) and echo times (TE), respectively. An inversion recovery (IR) turbo fast low-angle shot (FLASH) with magnitude reconstruction pulse sequence was performed for quantitative T_1 measurement. The raw data were acquired using a centric *k*-space reordering scheme, followed by the phase encoding steps with higher phase encoding gradient amplitudes. Data acquisition parameters of the FLASH readout were TR/TE/Flip angle = 10 ms/5 ms/10°. The standard multi-echo Carr-Purcell-Meiboom-Gill pulse sequence was used for measuring T_2 from a single echo train. The T_2 maps were obtained on a voxel-by-voxel basis using nonlinear least-squares fit the equation $M = M_0 e^{-TE/T_2}$ from the images taken at each echo time. All maps were processed using in-house MatLab scripts (MathWorks Inc., Natick, MA, USA).

Abbreviations

| | |
|----------------|---|
| MRI | Magnetic resonance imaging |
| MRS | Magnetic resonance spectroscopy |
| TR | Repetition time |
| TE | Echo time |
| NOESY | Nuclear overhauser effect spectroscopy |
| β -Gal | β -Galactosidase |
| PIH | Pyridoxal isonicotinoylhydrazone |
| SBH | Salicylaldehyde benzoylhydrazone |
| SIH | Salicylaldehyde isonicotinoylhydrazone |
| SNH | Salicylaldehyde nicotinoylhydrazone |
| <i>p</i> -FSBH | 2-Hydroxyl-5-fluoro-benzaldehyde benzoylhydrazone |
| SBHF- <i>p</i> | 2-Hydroxylbenzaldehyde 4-fluorobenzoylhydrazone |
| PRE | Paramagnetic relaxation enhancement |
| DMSO | Dimethyl sulfoxide |
| FAC | Ferric ammonium citrate |
| PBS | Phosphate buffered saline |
| TLC | Thin layer chromatography. |

Acknowledgements

This research was supported by the DOD Prostate Cancer New Investigator Award W81XWH-05-1-0593. NMR experiments were performed at the Advanced Imaging Research Center. We are grateful to Dr Ralph Mason for valuable discussion, Jennifer McAnally and Ya Ren for expert technical assistance.

References

- 1 A. Kruger, V. Schirrmacher and R. Khokha, *Cancer Metastasis Rev.*, 1999, **17**, 285.
- 2 U. Haberkorn, W. Mier and M. Eisenhut, *Curr. Med. Chem.*, 2005, **12**, 779.
- 3 A. Razgulin, N. Ma and J. H. Rao, *Chem. Soc. Rev.*, 2011, **40**, 4186.
- 4 L. Li, R. J. Zemp, G. Lungu, G. Stoica and L. V. Wang, *J. Biomed. Opt.*, 2007, **12**, 020504.
- 5 C. H. Tung, Q. Zeng, K. Shah, D. E. Kim, D. Schellingerhout and R. Weissleder, *Cancer Res.*, 2004, **64**, 1579.
- 6 M. Kamiya, H. Kobayashi, Y. Hama, Y. Koyama, M. Bernardo, T. Nagano, P. L. Choyke and Y. Urano, *J. Am. Chem. Soc.*, 2007, **129**, 3918.
- 7 V. Jossierand, I. Texier-Nogues, P. Huber, M. C. Favrot and J. L. Coll, *Gene Ther.*, 2007, **14**, 1587.
- 8 T. S. Wehrman, G. von Degenfeld, P. O. Krutzik, G. P. Nolan and H. M. Blau, *Nat. Methods*, 2006, **3**, 295.
- 9 L. Liu and R. P. Mason, *PLoS One*, 2010, **5**, e12024.
- 10 S. Celen, C. Deroose, T. de Groot, S. K. Chitneni, R. Gijssbers, Z. Debyser, L. Mortelmans, A. Verbruggen and G. Bormans, *Bioconjugate Chem.*, 2008, **19**, 441.
- 11 M. E. Van Dort, K. C. Lee, C. A. Hamilton, A. Rebemtulla and B. D. Ross, *Mol. Imaging*, 2008, **7**, 187.
- 12 A. Y. Louie, M. M. Huber, E. T. Ahrens, U. Rothbacher, R. Moats, R. E. Jacobs, S. E. Fraser and T. J. Meade, *Nat. Biotechnol.*, 2000, **18**, 321.
- 13 Y. T. Chang, C. M. Cheng, Y. Z. Su, W. T. Lee, J. S. Hsu, G. C. Liu, T. L. Cheng and Y. M. Wang, *Bioconjugate Chem.*, 2007, **18**, 1716.
- 14 K. Hanaoka, K. Kikuchi, T. Terai, T. Komatsu and T. Nagano, *Chem.–Eur. J.*, 2008, **14**, 987.
- 15 F. Arena, J. B. Singh, E. Gianolio, R. Stefania and S. Aime, *Bioconjugate Chem.*, 2011, **22**, 2625.
- 16 W. Cui, L. Liu, V. D. Kodibagkar and R. P. Mason, *Magn. Reson. Med.*, 2010, **64**, 66.
- 17 N. E. Bengtsson, G. Brown, E. W. Scott and G. W. Walter, *Magn. Reson. Med.*, 2010, **63**, 745.
- 18 J.-X. Yu, V. D. Kodibagkar, W. Cui and R. P. Mason, *Curr. Med. Chem.*, 2005, **12**, 819.
- 19 (a) J.-X. Yu, P. Otten, Z.-Y. Ma, W. Cui, L. Liu and R. P. Mason, *Bioconjugate Chem.*, 2004, **15**, 1334; (b) W. Cui, P. Otten, Y.-M. Li, K. S. Koeneman, J.-X. Yu and R. P. Mason, *Magn. Reson. Med.*, 2004, **51**, 616; (c) J.-X. Yu, Z.-Y. Ma, Y.-M. Li, K. S. Koeneman, L. Liu and R. P. Mason, *Med. Chem.*, 2005, **1**, 255; (d) J.-X. Yu, L. Liu, V. D. Kodibagkar, W. Cui and R. P. Mason, *Bioorg. Med. Chem.*, 2006, **14**, 326.
- 20 J.-X. Yu and R. P. Mason, *J. Med. Chem.*, 2006, **49**, 1991.
- 21 V. D. Kodibagkar, J.-X. Yu, L. Liu, H. Hetherington and R. P. Mason, *Magn. Reson. Imaging*, 2006, **24**, 959.
- 22 L. Liu, V. D. Kodibagkar, J.-X. Yu and R. P. Mason, *FASEB J.*, 2007, **21**, 2014.
- 23 J.-X. Yu, V. D. Kodibagkar, L. Liu and R. P. Mason, *Magn. Reson. Med.*, 2008, **21**, 704.
- 24 J.-X. Yu, W. Cui, D. Zhao and R. P. Mason, *Fluorine Health*, 2008, 197.
- 25 J.-X. Yu, V. D. Kodibagkar, R. R. Hallac, L. Liu and R. P. Mason, *Bioconjugate Chem.*, 2012, **23**, 596.
- 26 S. Mizukami, H. Matsushita, R. Takikawa, F. Sugihara, M. Shirakawa and K. Kikuchi, *Chem. Sci.*, 2011, **2**, 1151.
- 27 R. Weissleder and M. J. Pittet, *Nature*, 2008, **452**, 580.
- 28 (a) Y. Takaoka, T. Sakamoto, S. Tsukiji, M. Narazaki, T. Matsuda, H. Tochio, M. Shirakawa and I. Hamachi, *Nat. Chem.*, 2009, **1**, 557; (b) Y. Takaoka, Y. Sun, S. Tsukiji and I. Hamachi, *Chem. Sci.*, 2011, **2**, 511.
- 29 M. Ito, A. Shibata, J. Zhang, M. Hiroshima, Y. Sako, Y. Nakano, K. Kojima-Aikawa, B. Mannervik, S. Shuto, Y. Ito, R. Morgenstern and H. Abe, *ChemBioChem*, 2012, **13**, 1428.
- 30 (a) K. Mizusawa, Y. Ishida, Y. Takaoka, M. Miyagawa, S. Tsukiji and I. Hamachi, *J. Am. Chem. Soc.*, 2010, **132**, 7291; (b) Y. Takaoka, K. Kiminami, K. Mizusawa, K. Matsuo, M. Narazaki, T. Matsuda and I. Hamachi, *J. Am. Chem. Soc.*, 2011, **133**, 11725.
- 31 P. Harvey, K. H. Chalmers, E. De Luca, A. Mishra and D. Parker, *Chem.–Eur. J.*, 2012, **18**, 8748.
- 32 M. Higuchi, N. Iwata, Y. Matsuba, K. Sato, K. Sasamoto and T. C. Saido, *Nat. Neurosci.*, 2005, **8**, 527.
- 33 K. Yamaguchi, R. Ueki, H. Nonaka, F. Sugihara, T. Matsuda and S. Sando, *J. Am. Chem. Soc.*, 2011, **133**, 14208.
- 34 S. Mizukami, R. Takikawa, F. Sugihara, Y. Hori, H. Tochio, M. Walchli, M. Shirakawa and K. Kikuchi, *J. Am. Chem. Soc.*, 2008, **130**, 794.

- 35 (a) S. Mizukami, R. Takikawa, F. Sugihara, M. Shirakawa and K. Kikuchi, *Angew. Chem., Int. Ed.*, 2009, **48**, 3641; (b) H. Matsushita, S. Mizukami, Y. Mori, F. Sugihara, M. Shirakawa, Y. Yoshioka and K. Kikuchi, *ChemBioChem*, 2012, **13**, 1579.
- 36 K. Tanaka, N. Kitamura and Y. Chujo, *Bioconjugate Chem.*, 2011, **22**, 1484.
- 37 M. Srinivas, A. Heerschap, E. T. Ahrens, C. G. Figdor and I. J. M. de Vries, *Trends Biotechnol.*, 2010, **28**, 363.
- 38 E. T. Ahrens, R. Flores, H. Y. Xu and P. A. Morel, *Nat. Biotechnol.*, 2005, **23**, 983.
- 39 D. G. Reid and P. S. Murphy, *Drug Discovery Today*, 2008, **13**, 473.
- 40 (a) D. Zu and R. C. Hider, *Coord. Chem. Rev.*, 2002, **232**, 151; (b) J. L. Buss, B. T. Greene, J. Turner, F. M. Torti and S. V. Torti, *Curr. Top. Med. Chem.*, 2004, **4**, 1623.
- 41 (a) D. B. Lovejoy and D. R. Richardson, *Curr. Med. Chem.*, 2003, **10**, 1035; (b) D. R. Richardson, *Curr. Med. Chem.*, 2005, **12**, 2711; (c) D. S. Kalinowski and D. R. Richardson, *Pharmacol. Rev.*, 2005, **57**, 547; (d) D. R. Richardson, D. S. Kalinowski, S. Lau, P. J. Jansson and D. B. Lovejoy, *Biochim. Biophys. Acta, Gen. Subj.*, 2009, **1790**, 702.
- 42 (a) N. Richardson and J. A. Davies, *Polyhedron*, 1999, **18**, 2457; (b) D. D. Schwert, J. A. Davies and N. Richardson, *Top. Curr. Chem.*, 2002, **221**, 165.
- 43 G. M. Clore and J. Iwahara, *Chem. Rev.*, 2009, **109**, 4108.
- 44 (a) K. H. Chalmers, E. De Luca, N. H. M. Hogg, A. M. Kenwright, I. Kuprov, D. Parker, M. Botta, J. I. Wilson and A. M. Blamire, *Chem.–Eur. J.*, 2010, **16**, 134; (b) K. H. Chalmers, A. M. Kenwright, D. Parker and A. M. Blamire, *Magn. Reson. Med.*, 2011, **66**, 931; (c) P. Harvey, I. Kuprov and D. Parker, *Eur. J. Inorg. Chem.*, 2012, 2015; (d) F. Schmid, C. Holtke, D. Parker and C. Faber, *Magn. Reson. Med.*, 2012, **66**, 931.
- 45 G. H. Bao, M. Clifton, T. M. Hoette, K. Mori, S. X. Deng, A. Qiu, M. Viltard, D. Williams, N. Paragas, T. Leete, R. Kulkarni, X. Li, B. Lee, A. Kalandadze, A. J. Ratner, J. C. Pizarro, K. M. Schmidt-Ott, D. W. Landry, K. N. Raymond, R. K. Strong and J. Barasch, *Nat. Chem. Biol.*, 2010, **6**, 602.
- 46 J. A. Davies, S. G. Dutremez, C. M. Hockensmith, R. Keck, N. Richardson, S. Selman, D. A. Smith, C. W. Ulmer II, L. S. Wheatley and J. Zeiss, *Acad. Radiol.*, 1996, **3**, 936.
- 47 D. D. Schwert, N. Richardson, G. Ji, B. Raduchel, W. Ebert, P. E. Heffner, R. Keck and J. A. Davies, *J. Med. Chem.*, 2005, **48**, 7482.
- 48 J.-X. Yu, P. K. Gulaka, L. Liu, V. D. Kodibagkar and R. P. Mason, *ChemPlusChem*, 2012, **77**, 370.
- 49 K. L. Haas and K. J. Franz, *Chem. Rev.*, 2009, **109**, 4921.
- 50 (a) X. Chen, B. Wu and P. G. Wang, *Curr. Med. Chem.: Anti-Cancer Agents*, 2003, **3**, 139; (b) Y. Singh, M. Palombo and P. J. Sinko, *Curr. Med. Chem.*, 2008, **15**, 1802; (c) F. Kratz, I. A. Müller, C. Ryppa and A. Warnecke, *ChemMedChem*, 2008, **3**, 20.
- 51 O. Coskuner and C. A. Gonzalez, *Metallic Systems: A Quantum Chemists Perspective, Chapter 3, Carbohydrate and Trivalent Iron Ion Interactions*, ed. T. C. Allison, O. Coskuner and C. A. Gonzalez, CRC Press, Taylor & Francis Group, 2011, pp. 83–106, ISBN: 1420060775, 9781420060775.